Journal of South American Earth Sciences 108 (2021) 103179

Contents lists available at ScienceDirect

Journal of South American Earth Sciences

journal homepage: www.elsevier.com/locate/jsames

DInSAR and statistical modeling to assess landslides: The case study of Sierras Chicas (central Argentina)

Almendra Brasca Merlín [a,b,c], Andrés Solarte [a,b,d], Laura M. Bellis [a,b,d], Claudio Carignano [b,e], Marcela Cioccale [b], Manuel Delgado [a], Marcelo Scavuzzo [a], Juan P. Argañaraz [a,d,*]

[a] Instituto de Altos Estudios Espaciales "Mario Gulich" (CONAE-UNC), Ruta C45, Km 8, CP, 5187, Falda Del Cañete, Córdoba, Argentina
[b] Facultad de Ciencias Exactas Físicas y Naturales, Universidad Nacional de Córdoba, Av. Vélez Sarsfield 1611, CP, 5000, Córdoba, Argentina
[c] Secretaría de Ciencia y Técnica, Universidad Nacional de Córdoba. Juan Filloy S/n, Ciudad Universitaria, CP, 5000, Córdoba, Argentina
[d] Consejo Nacional de Investigaciones Científicas y Técnicas (CONICET), Argentina
[e] Centro de Investigaciones en Ciencias de La Tierra (CICTERRA, CONICET-UNC), Av. Vélez Sarsfield 1611, CP, X5016GCA, Córdoba, Argentina

ARTICLE INFO

Keywords:
Remote sensing
DInSAR
Cosmo-SkyMed
Sentinel-1
Landslides
Wildfires
Sierras pampeanas
Córdoba province

ABSTRACT

The main goal of this investigation was to assess landslides in the steep West-facing slope of the *Sierras Chicas* mountains in central Argentina using two complementary approaches: Differential SAR interferometry (DinSAR) and statistical modeling. The combination of the geological characteristics of the area, wildfires, intense rainfall events and human disturbances have made the area highly susceptible to landslides. This condition has been recently aggravated with the construction of a roadway. In this work, we applied DInSAR methods to explore the suitability of COSMO-SkyMed (CSK) acquisitions to measure displacements and we used Sentinel-1 C-band images for accuracy comparison. In addition, Generalized Linear Models were fitted to identify landslide-conditioning factors. Based on the results obtained, Sentinel-1 proved to be the most adequate source of images to perform interferometry, in contrast to Cosmo Skymed imagery that showed very poor coherence in the study area. The statistical modeling identified slope degree, distance to roads and fire frequency as the main variables explaining landslide occurrence on the west escarpment of the Sierras Chicas. Results will hopefully contribute to improving future applications of SAR interferometry both in the study area and others with similar characteristics, as well as the tools and knowledge for decision making in engineering and urban development projects in order to minimize risk.

1. Introduction

The Earth's surface is under constant change and landslides are one of the most common manifestations of ground movement. These deformations and mass removal events are the result of a complex interaction of geological, geomorphological, hydrogeological, climatic and ecological conditions as well as manmade structures (García-Ruiz et al., 2010; Gorsevski et al., 2006; Highland and Bobrowsky, 2008; Rozos et al., 2008). They represent a significant geological hazard worldwide, sometimes causing damage to infrastructures, great number of casualties in urban areas and severe damage to ecosystems (Bianchini et al., 2015; Moreiras and Coronato, 2009; Nutricato et al., 2015). Therefore, studies aiming at monitoring land surface displacements and understanding the conditions under which landslides are more likely to occur are of great importance to minimize risk.

Remote Sensing and Geographic Information Systems (GIS) technology constitute powerful tools for landslide monitoring and hazard assessment. In particular, Differential Interferometry Synthetic Aperture Radar (DInSAR) has been successfully applied to measure land deformations. The launch of satellites with SAR sensors such as COSMO-SkyMed, operating at 3.1 cm wavelength in X-band, and Sentinel-1, operating at 5.54 cm wavelength in C-band, have significantly improved the ability to detect millimetric displacements. Such results are useful to update and improve landslide datasets over large areas, detecting changes in displacement velocities and providing significant advances to the understanding of landslide conditioning factors (Barra

* Corresponding author. Instituto de Altos Estudios Espaciales "Mario Gulich" (CONAE-UNC), Ruta C45, Km 8, CP, 5187, Falda Del Cañete, Córdoba, Argentina.
E-mail addresses: abrascamerlin@unc.edu.ar (A. Brasca Merlín), asolarte@fundacionkittl.org.ar (A. Solarte), lbellis7@gmail.com (L.M. Bellis), ccarignano@unc.edu.ar (C. Carignano), mcioccale@unc.edu.ar (M. Cioccale), delgado.manuel@outlook.com (M. Delgado), scavuzzo@conae.gov.ar (M. Scavuzzo), jparganaraz@unc.edu.ar (J.P. Argañaraz).

https://doi.org/10.1016/j.jsames.2021.103179
Received 10 April 2020; Received in revised form 7 January 2021; Accepted 14 January 2021
Available online 4 February 2021

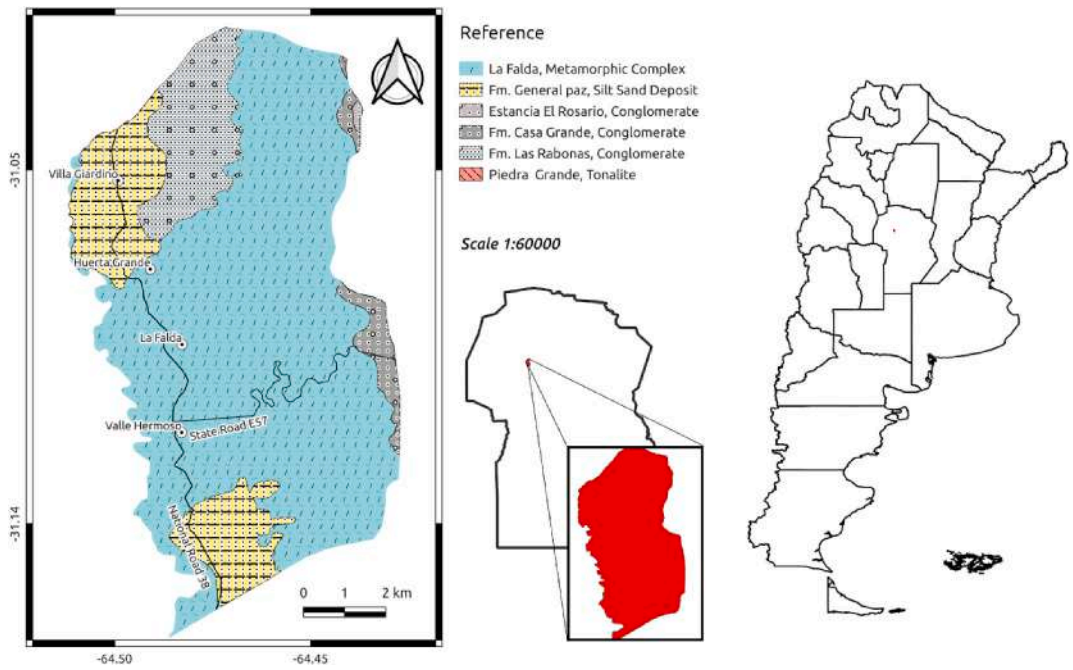

Fig. 1. Location and lithology of the study area in the western hillside of the Sierras Chicas of Córdoba Province, in central Argentina. The boundaries of Córdoba Province are in the smaller central image (black boundaries) and the red polygon highlights the study area (9100 ha).

et al., 2016; Calò et al., 2014; Di Martire et al., 2016; Herrera et al., 2013; Infante et al., 2019; Pappalardo et al., 2018).

Besides DInSAR methods, further complementary studies can be carried out to improve our understanding of landslide conditioning factors. Statistical modeling allows defining quantitative relationships between the spatial distribution of a set of environmental variables and the occurrence of historical landslides (Chen et al., 2017; Conoscenti et al., 2015; Youssef et al., 2016; Zêzere et al., 2017). These environmental variables may include topography (e.g. slope steepness, aspect, elevation, curvature), geology (e.g. rock types, distance to faults, structural aspects), hydrology (e.g. distance to streams and soil moisture) and land use/land cover (e.g. roads, type of vegetation, wildfires). A better understanding of the conditions associated with landslides will lead to accurate predictions, as to where landslides are more likely to occur, and the adoption of management regulations to reduce hazard (Zhang et al., 2016).

In this work, we applied DInSAR methods to explore the suitability of COSMO-SkyMed (CSK) acquisitions to measure displacements on the steep west-facing slope of the Sierras Chicas mountains in central Argentina. Several landslide events have been registered in this area in the last few years, most of them related to the construction of a mountain road, locally known as *El Cuadrado*. One of the main advantages of CSK imagery is their high spatial resolution that allows more detailed displacement measurements. Moreover, the SAR instrument works in a high frequency spectrum (X Band), which makes it more sensitive to small terrain motions (Hanssen, 2001). However, our analysis was conditioned by a limited number of acquisitions within the same beam, and we applied DInSAR techniques to pairs of CSK imagery. In addition, we used the same approach with Sentinel 1 images of the same period, in order to validate results and compare their suitability. Along with DInSAR techniques, we studied the environmental conditions under which historical landslides occurred in our study area using statistical modeling. To the best of our knowledge, this study represents the first application of Differential SAR Interferometry to address land deformation monitoring in the *Sierras Pampeanas,* and it is the first attempt to identify landslide-conditioning factors in this area using Remote Sensing and GIS derived data.

2. Study area

The study area covers a portion of the west facing slope of *Sierras Chicas* mountains of Córdoba (eastern Sierras Pampeanas) in central Argentina, including El Cuadrado road and its surroundings (9100 ha, Fig. 1), where numerous landslide events occurred after the road was constructed. *Sierras Chicas* extend north-south for about 200 km (30° 36′ S and 32° 38′S) and east-west nearly 15 km (Carignano et al., 2014), with an altitudinal range between 500 and 1949 m a.s.l. Climate is temperate semi arid, with a monsoonal rain regime. The average annual rainfall is 850 mm, occurring mainly between October and March (spring and summer) and the mean annual temperature is 17.3° (National Meteorological Service of Argentina, data from 1999 to 2014). These mountains belong to the Chaco Serrano phytogeographical subregion, and vegetation consists of a mosaic of forests, shrublands and grasslands. Native forests and shrublands are more abundant at lower elevations (<900 m a.s.l.) and grasslands dominate elevations above 900 m a.s.l. (Cabido et al., 2018; Giorgis et al., 2017).

Sierras Chicas present a steep western hillside, generated by the Punilla Fault, which raises the base block above the Punilla and Calamuchita valleys. The main lithology corresponds to gneisses and tonalite-biotytic schist of pre-Cambrian age (>2500 Ma), intruded by numerous igneous bodies of Eopaleozoic age (542 Ma) (Lencinas, 1971) (Fig. 1). The hillside is composed of foliated metamorphosed and fractured rock with differential weathering degree along fracture zones (Carignano et al., 2014). Neotectonic activity is intense in the area (Martino et al., 2012; Massabie et al., 2003), with frequent shallow seismic events of low to medium magnitude (Richardson et al., 2012) and few events of great magnitude (Carignano et al., 2014). These seismic movements together with intense rainfall events are the main triggering factors of landslide activity in the Sierras Chicas (Beltramone, 2005; Moreiras and Coronato, 2009).

The characterized landslides can be classified as translational, rotational, debris flow, slump, creeping and rock fall according to Varnes (1978). These landslides had well marked lobes and large magnified takeoff cracks, and a generalized tendency of the slope to creeping (Figure S1). The high degree of fracturation of the igneous-metamorphic rocks (Lencinas, 1971), due to the proximity to the Punilla fault and

Table 1
Incidence angles, number and period of acquisition of the Cosmo-SkyMed and Sentinel-1B images processed with Differential Interferometry to assess displacements on the west hillside of the Sierras Chicas mountains in central Argentina.

Sensor	Beam or swath	Incidence Angle	Number of acquisitions and range of dates
CSK	H-01	22.6°–25.7°	8 (05/2016–11/2016)
	H-07	32.43°–34.43°	2 (02/2017–04/2017)
	H-13	39.34°–41.39°	6 (01/2017–05/2017)
	H-18	45.7°–46.8°	5 (05/2016–02/2017)
S–1B	IW2	36.47°–41.85°	3 (04/2016–09/2016)

weathering processes, is considered one of the main conditioning factors (Figure S2). Several landslide events, such as rock falls, slides and debris flows were triggered after intense rainstorms. To the north end of the *Sierras Chicas*, on the western hillslope of Cerro Uritorco peak (1949 m a.s.l.), a megalandslide was identified, probably triggered by an intense earthquake, in combination with the above-mentioned lithological characteristics, regional structures and climatic events (Carignano et al., 2014).

3. Materials and methods

3.1. Differential SAR interferometry applied to Cosmo-SkyMed and Sentinel-1

In order to study displacements by means of SAR images, we applied Differential Interferometry to pairs of Cosmo-SkyMed (CSK) and Sentinel 1 imagery. We had access to 20 CSK SAR images acquired between 2016 and 2017 in four different beams for our study area (Table 1, Fig. 2). We used images acquired on stripmap mode, HIMAGE parameter, 3 m of geometric resolution, sensor height of 620 km, simple polarization and swath width of 40 × 40 km. Single Look Complex Slant (SLC/L1A) specific level was chosen, which corresponds to images in oblique range and complex format. In addition to CSK imagery, we processed Sentinel-1B Level-1 SLC (S1), dual polarization from April 2016 to September 2016 (Table 1, Fig. 2) to assess the accuracy of the DinSAR method applied to CSK and to compare the suitability of both sensors. Only descending orbit CSK pairs were available for our study area, and the equivalents for S1 were sought. Another optimistic feature of S1 is the accuracy of its orbit, which could improve a possible failure in the CSK data. Images were processed with Scientific Computing Environment, *ISCE* (CSK) and Sentinel Application Platform, *SNAP* (S1).

The suitability of all possible pairs of images within a beam to generate an interferogram was assessed by the perpendicular baseline. In the resulting maps, we used a coherence threshold of 0.25 to mask out non-coherent pixels (Zhao et al., 2016). The interferometric coherence is a statistical measure of the phase stability between two dates. Coherence ranges from 0 to 1; 0 indicating that the interferometric phase is just noise, and 1 complete absence of phase noise.

To evaluate what generates the changes in the coherence between the acquisitions, the critical baseline is analyzed based on the formula proposed by Hanssen (2001), considering an average slope for the area of interest of 30°, which certifies that the geometric correlation coefficient is not linked to the final product to be detailed below.

3.2. Landslide conditioning factors

We analyzed landslide conditioning factors using GLM (Generalized Linear Models) with binomial response and logit link function (Quinn and Keough, 2002). We used an updated version of the landslide database from Brasca Merlin et al. (2018), derived through interpretation of high resolution Google Earth and Bing Maps imagery (last access on February 2020), and SPARTAN aerial photos acquired in 1970 (1:22,000) and 1987 (1:35,000). The database was complemented with field campaigns in 2014 and 2015. Sixty landslides were registered with an average size of 65,563 m^2 (Fig. 3). As in Gorsevsky et al. (2006), the area of initiation of each landslide was interpreted as the point representing the presence of a landslide, which proved to be accurate in comparison to other strategies of representing landslide occurrence (Zêzere et al., 2017). In order to have the same proportion of presence and absence data, we randomly created 60 points to get the non-landslide dataset (Youssef, 2015). The non-landslide points had a minimum separation of 150 m among them and were at least 90 m apart from the delineated landslide polygons.

The pool of independent data for GLM fitting was created based on previous literature and disturbances affecting our study area (e.g.

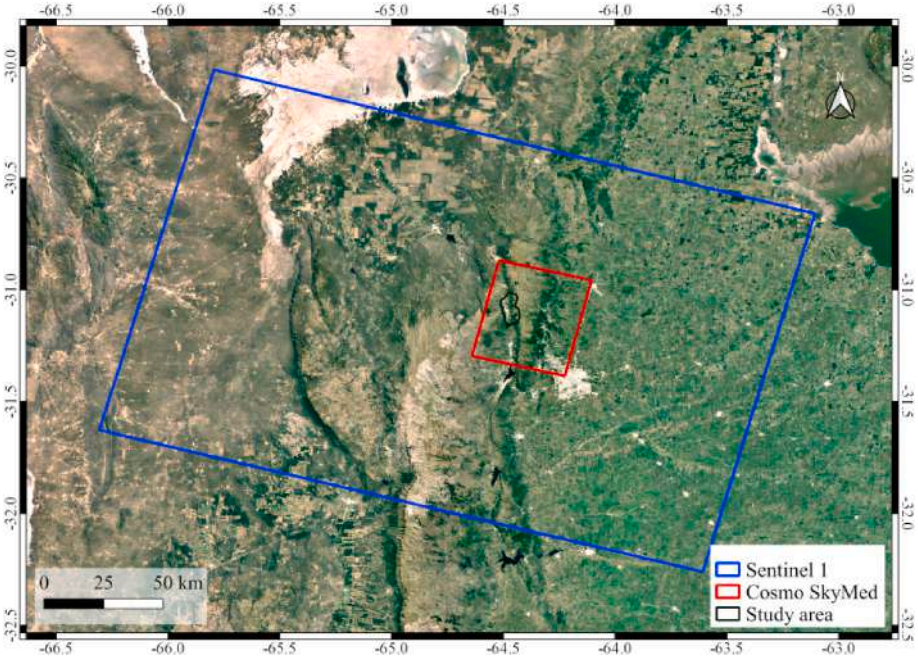

Fig. 2. The acquisition coverage area of Cosmo SkyMed and Sentinel 1 imagery.

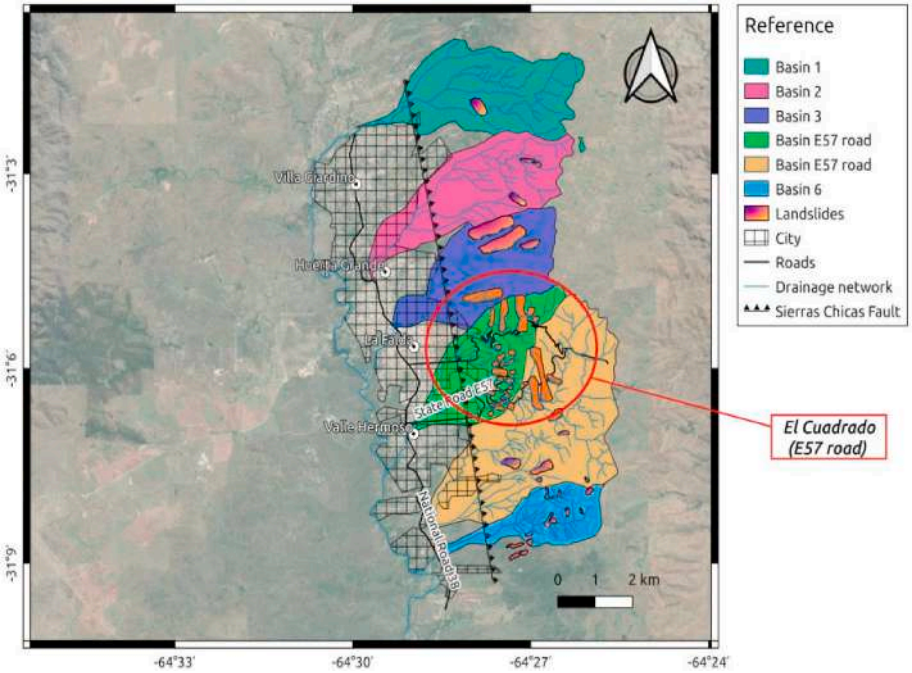

Fig. 3. Landslide database for El Cuadrado road (E57) and its surroundings on the west hillside of the Sierras Chicas of Córdoba province, central Argentina.

Table 2
Summary of data analysis obtained for Cosmo-SkyMed imagery (beam 01, year 2016) on the West hillside of the Sierras Chicas mountains in central Argentina.

Pair	Perpendicular baseline (m)	Critical baseline (m)	Geometric correlation coefficient[a]	Days between acquisitions
May 15 - July 07	256.6	13215.6	0.9806	60
July 14 - Oct 02	69.4	13214.1	0.9947	80
July 31 - Sept 16	253.5	13217.1	0.9808	47
July 31 - Oct 10	140.1	13217.1	0.9894	71
Sept 01 - Sept 16	307.2	13213.3	0.9768	15
Sept 16 - Oct 10	117.1	13213.3	0.9911	24

[a] Geometric correlation coefficient is obtained as (B_critical - B_perp)/B_crit being **B_crit** the theoretic critical baseline for a given pair and **B_perp** the perpendicular baseline estimated for that pair.

Table 3
Summary of data analysis obtained for Sentinel 1 imagery (IW2, year 2016) on the West hillside of the Sierras Chicas mountains in central Argentina.

Pair	Perpendicular baseline (m)	Critical baseline (m)	Geometric correlation coefficient	Days between acquisitions
April 17 - May 11	27.5	18,692,4	0.9985	24
May 11 - June 28	3.3	18,701,2	0.9998	48
June 28 - July 22	123.4	18,701,2	0.9934	24
July 22 - August 15	74.5	18,692,4	0.9960	24
August 15 - Sept 08	3.2	18,692,4	0.9998	24

Argañaraz et al., 2015; Beltramone, 2005; Chen et al., 2017; Gorsevski et al., 2006; Zhang et al., 2016). We selected 15 landslide conditioning factors, including elevation, slope steepness, aspect, lithology, profile convexity, plain convexity, longitudinal convexity, cross sectional convexity, minimum curvature, maximum curvature, land cover, fire frequency and distance to faults, roads and streams.

Topographic variables were derived from a Digital Elevation Model with a spatial resolution of 5 m (Argentinian National Geographic Institute, IGN). The aspect was reclassified in 4 directional classes (N, S, E, W) instead of the 8 classes mostly used in literature to reduce the degrees of freedom when fitting the model. The road network was obtained from IDECOR (Infrastructure for Spatial Information of Córdoba Province, available at https://www.mapascordoba.gob.ar/, accessed on December 15, 2019), using first order roads. The drainage network was derived by visual interpretation of high-resolution imagery and contour and slope lines (Fig. 3). Distance rasters were derived at 10 m spatial resolution.

The land cover map was obtained from a multitemporal classification of Landsat 8 OLI images acquired on April 16 and August 6, 2013 (30 m spatial resolution, path/row: 229/82). A supervised classification was performed using Support Vector Machines, obtaining an overall accuracy of 93.8% (for further details see Argañaraz et al., 2018). The fire database from the 1986–2017 period was derived from Landsat TM, ETM+ and OLI imagery (30 m, path/row: 229/82). We used the same fire database as in Argañaraz et al. (2015), in which burned scars from 1999 to 2011 were extracted using a two-phase algorithm, consisting of identifying burned seeds first, and then applying a region growing algorithm to delineate the boundaries of the burned areas (Bastarrika et al., 2011). For the remaining period, we used an updated version of the Burned Area Mapping Tool (*BAMT*, Bastarrika et al., 2014) implemented in Google Earth Engine (GEE). BAMS algorithm proved to be efficient in delineating burned areas in Córdoba mountains, with

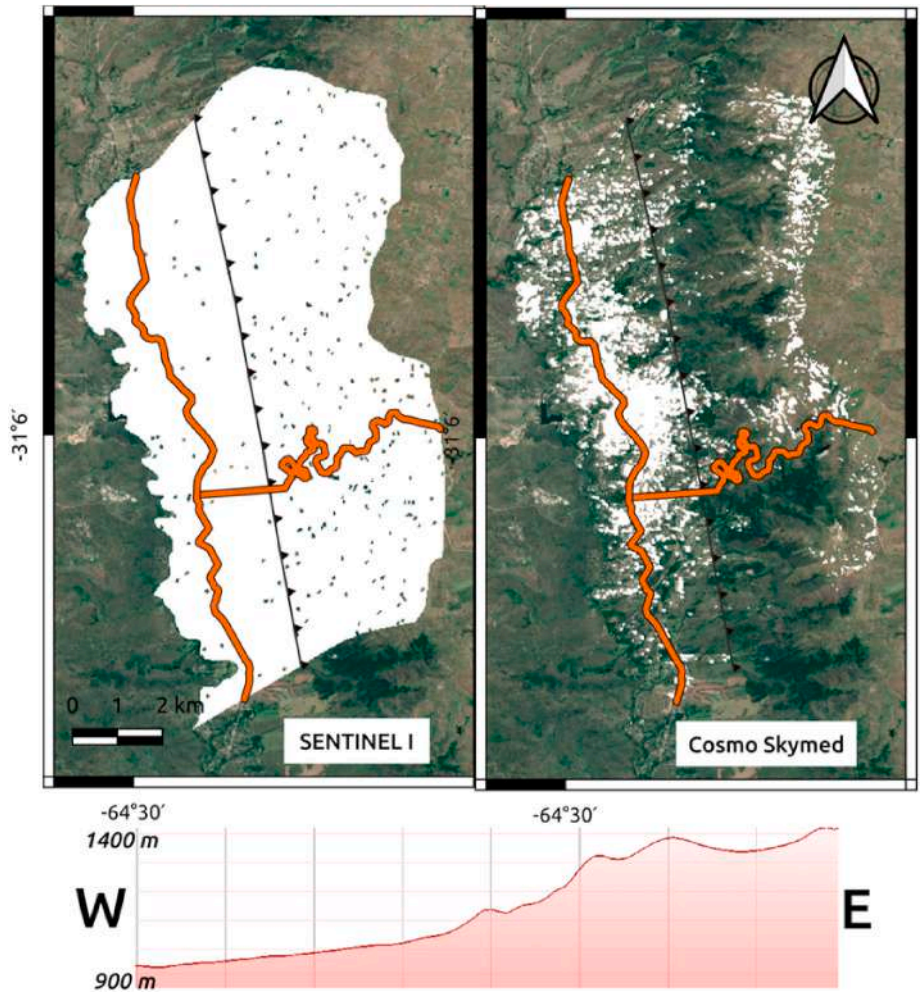

Fig. 4. Coherence masks generated for Sentinel-1 and Cosmo Skymed data, based on the 0.25 threshold. All pixels below this threshold in any pair were masked.

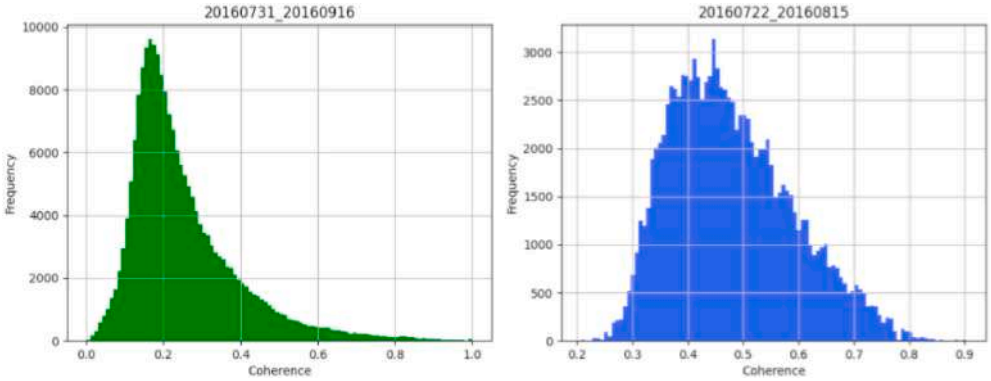

Fig. 5. Distribution of coherence values for pairs of Cosmo-SkyMed (left) and Sentinel-1 (right) corresponding to a similar period (CSK: 2016-07-31 - 2016-09-16; Sentinel 1:2016–07-22 - 2016-08-15).

omission and commission errors lower than 12% (Argañaraz et al., 2015; unpublished data).

Before performing the statistical analyses, the pool of independent variables was tested for multicollinearity using the spearman test, and we removed variables having $|r| \geq 0.7$. Afterwards, the 120-point dataset of landslides presence and absence was split to train (70%) and validate (30%) the model. The logistic regression model was fitted following a stepwise procedure, considering both directions, forward and backward, and using the step function of the Stats package in R (R Core Team, 2020). We ran full and reduced models to estimate the probability of landslide occurrence in relation to the set of independent variables selected. Model selection was carried out using the Akaike Information Criterion (AIC) (Quinn and Keough, 2002).

Acknowledging the limitations of stepwise selection procedures, we also performed a best subset analysis to identify landslide-conditioning factors, which compares all possible models using a specified set of predictors (Quinn and Keough, 2002). In this approach, we considered the best 10 models based on the Bayesian Information Criterion (BIC).

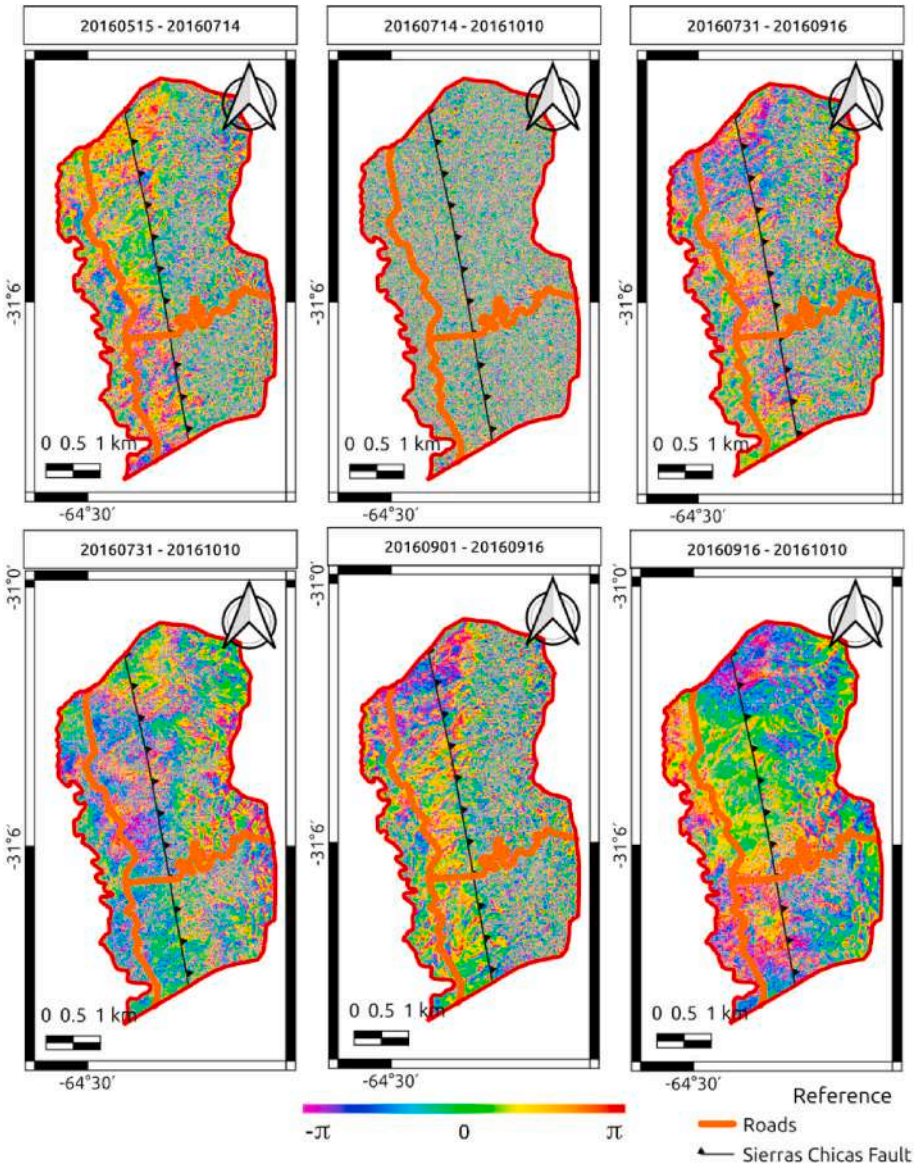

Fig. 6. Interferometric phase of CSK images.

The number of times each variable was included in those 10 models indicated its importance to explain landslide probability.

The predictive performance of the logistic regression model (30% validation data) and its fit to the training data were evaluated using the Receiver Operating Characteristic (ROC) curve (Lasko et al., 2005). In the ROC curve, the sensitivity of the model (true positive rate) is plotted against 1-specificity (false positive rate) for all possible cut-off values. The area under the ROC curve (AUC) represents the performance of the model to predict the occurrence or non-occurrence of landslides reliably. AUC values higher than 0.7 are considered acceptable, higher than 0.8 are considered excellent and higher than 0.9 are considered outstanding (Hosmer and Lemeshow, 2000). All statistical analyses were performed using R (R Core Team, 2020).

4. Results

4.1. Differential SAR interferometry

Based on the interferometric coherence maps and perpendicular baselines of the CSK set of images, the ones from beam 01 were the most suitable to generate interferograms. With this setting, the highest coherence results were obtained, although this beam showed a higher proportion of layover distortions in comparison to the other beams. In addition, the number of images available from this beam was higher (8 acquisitions), which is desired in these kinds of studies. Therefore, we analyzed 28 possible interferometric pairs, from which 6 fulfilled our coherence threshold (>0.25) and perpendicular baseline criteria. (Table 2).

The CSK imagery processing was not suitable for the identification of displacements in *Sierras Chicas* due to the low coherence of the interferometric pairs. On the other hand, the Sentinel-1 interferometric pairs showed better coherence, smaller perpendicular baselines and better revisit time, resulting in a considerably better theoretical accuracy measurement, despite their lower resolution. Nevertheless, as the study area had no landslides or appreciable movement during the acquisition period, no displacement could be measured with Sentinel-1 imagery. Table 3 summarizes the same analysis for S1.

CSK pairs show very low coherence, especially on the steepest slopes, as it can be seen in Fig. 4, where the pixels with coherence lower than 0.25 in any pair of images were masked. Instead, S1 pairs show higher coherence than 0.25 in most of our study area (Fig. 4). Geometric correlation coefficients were not different between S1 and CSK data.

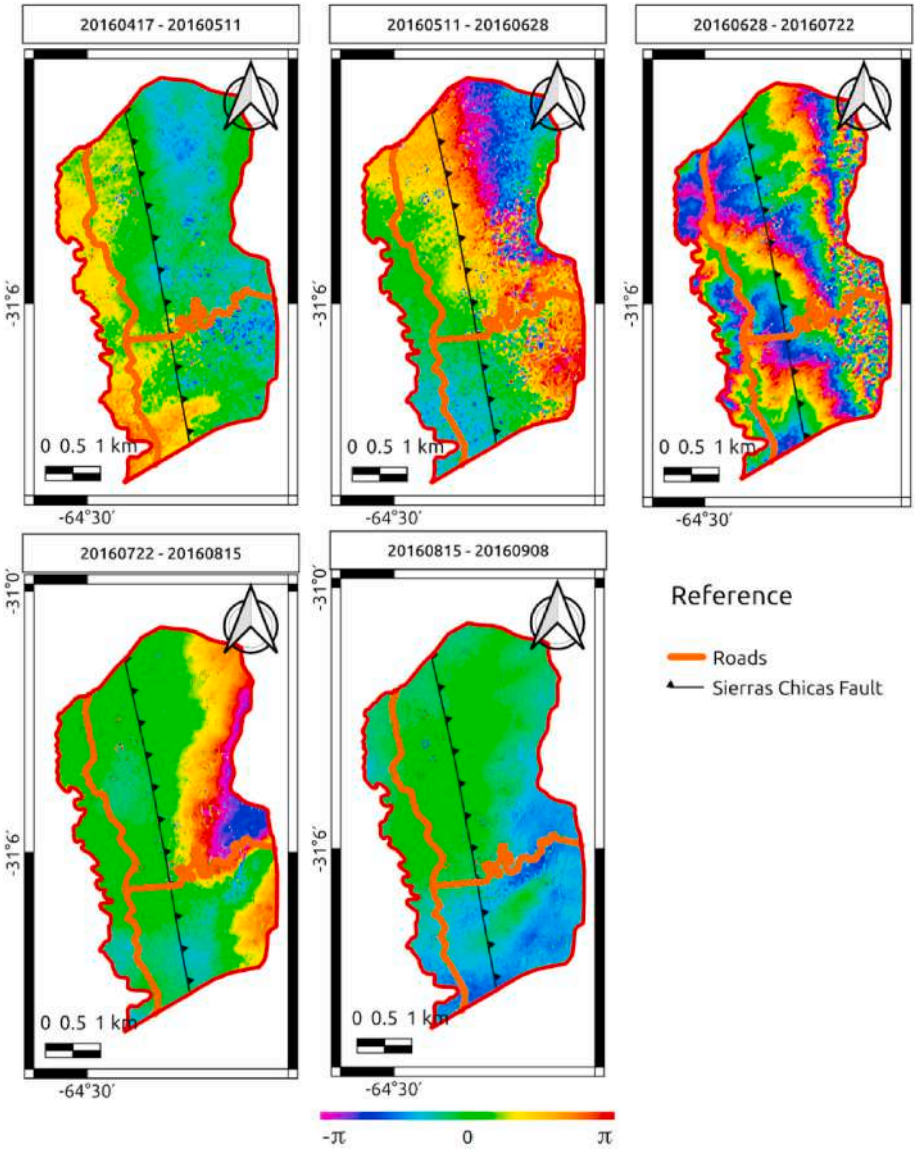

Fig. 7. Interferometric phase of S1 images.

Perpendicular baselines in S1 images are much lower than the CSK ones with a similar critical baseline (Tables 2 and 3). This means that the low coherence values of Cosmo-Skymed images are a product of temporal decorrelation between images. As CSK sensor operates with a smaller wavelength than S1 the changes of vegetation on the hillside through the year affect more CSK than S1 images.

The comparison of displacement measurements could not be performed due to the lack of useful data from CSK, and S1 images were used to compare the coherence of C-band in the study area. Fig. 5 shows the coherence distributions for two pairs of CSK and S1 corresponding to a similar period of time, in which higher coherence values can be appreciated for S1 than for CSK. To support data analysis, Figs. 6 and 7 show the interferometric phase in CSK images and S1 images, respectively.

4.2. Landslide conditioning factors

The stepwise logistic regression model identified both human and topographic variables as conditioning factors of landslide occurrence. Fire frequency, distance to roads and slope steepness significantly explained landslide probability, while the distance to the fault was close to significance ($p = 0.0595$; Table 4, Fig. 8). Landslides were more likely to occur at steeper slopes, close to roads and in areas with frequent fires. Nagelkerke's pseudo R^2 indicated that this model explained 50% of the variation in landslide probability. The ROC curves showed a very good performance of the model, with AUC being 0.86 and 0.84 for the training and testing dataset, respectively.

The best subset analysis agreed well with the stepwise procedure, with fire frequency appearing in all the 10 best models, followed by distance to roads (six times), distance to fault (five times) and slope steepness (four times). Additionally, lithology appeared in two of the best models, although it was not significant in the stepwise logistic regression (Table 4, Fig. 9).

5. Discussion

5.1. Differential SAR interferometry

In this study, we explored the suitability of Cosmo-SkyMed interferometric pairs to detect displacements on the steep west-facing slope of the Sierras Chicas mountains in central Argentina. To the best of our knowledge, this study represents the first application of Differential SAR Interferometry to address land deformation monitoring in the *Sierras*

Table 4
Coefficients and significance of landslide conditioning factors in Sierras Chicas (central Argentina) obtained with logistic regression models. The reduced model was fitted using stepwise selection in both directions.

Model	Variables	Coefficient	Standard error	Pr > ChiSq	AIC	R2 (%)
Full	Intercept	−15.9300	2152.00		91.4	53.2
	Stream distance (m)	−0.0013	0.0026	**0.0154**		
	Road distance (m)	−0.0005	0.0002	**0.0082**		
	Fault distance (m)	−0.0006	0.0005	0.8876		
	Fire frequency	0.8362	0.3081	**<0.0001**		
	Slope degree	0.0463	0.0299	**0.0447**		
	Aspect: N	−0.3606	1.6380	0.6781		
	Aspect: W	−0.9735	1.2480			
	Aspect: S	−1.0810	1.5530			
	Lithology: NPegP	15.8300	2152.00	0.6211		
	Lithology: Q1a	1.0780	3018.00			
	Profile convexity	0.0004	0.0010	0.7067		
Reduced	Intercept	−1.0894	0.7851		80.0	50.4
	Fire frequency	0.8436	0.2542	**0.0009**		
	Fault distance (m)	−0.0008	0.0004	0.0595		
	Road distance (m)	−0.0005	0.0002	**0.0307**		
	Slope degree	0.0473	0.0233	**0.0424**		

Significant values are highlighted in bold ($p < 0.05$).

Pampeanas with DInSAR techniques. Our results indicated that CSK data was not suitable to measure displacements in our study area. The achieved coherence in escarpment areas was very low to interpret the displacement product properly. This problem might be compensated for by using a greater number of acquisitions over a longer period of time. However, the fact that CSK data on Sierras Chicas was acquired with different beams, did not allow forming sufficient interferometric pairs for a multitemporal analysis. Table 1 details the number of CSK acquisitions that could be grouped together to generate interferometric pairs according to the beam. The use of S1 in this work serves to support the characteristics of the relief with respect to a sensor as well as analyze if the wavelength detail is conducive to the relief. Sentinel 1 shows better results in terms of coherence and geometric correlation coefficient but requires further processing to assess the measured displacement.

Several circumstances may compromise the accuracy of DInSAR measurements. Phase unwrapping is a key step in the process of building the displacement map, in addition to the fact that our study area showed highly variable coherence values. Problems related to excessive precipitation and earthquakes were discarded based on field data provided by a local weather station located within the study area and regional seismic activity (data not shown). Errors in the acquisition geometry and the digital elevation model (DEM) were also disregarded. The environmental settings of our study area, characterized by a steep escarpment and dense vegetation, especially on the escarpment where forests are less disturbed by fire, logging and herbivory, were not ideal for the application of DInSAR techniques. In addition, unfavorable slope orientations with respect to the radar sensor acquisition geometry affects measurements because the direction of movements occur at slope angles opposite to the measurement capability of the sensor (Colesanti and Wasowski, 2004). The heterogeneous temporal distribution of acquisitions and short temporal extent of images in our stacks (Table 1) might also turn measurements less reliable, because of the existence of phase atmospheric artifacts that can only be compensated for with large multitemporal stacks (Wasowski and Bovenga, 2014).

Our analysis of land displacements with CSK was also conditioned by the limited number of compatible acquisitions freely available for our study area, i.e., their angle was variable. This prevented us from correcting errors by building longer time series of CSK imagery and applying more sophisticated techniques, such as Small Baseline Subset (SBAS) or Persistent Scatterer (PS) (Hooper, 2008). Instead, Sentinel 1 offers freely available imagery with consistent acquisition angles allowing building long time series. Although our DInSAR analysis with S1 provided more coherent results than CSK, displacement measurements were too high. It would be worthy to explore further DInSAR analyses with S1, building a longer time series than the one used in this work and more accurate techniques (Kampes, 2006; Idrees et al., 2013). In addition, the recently available SAR imagery from SAOCOM L-band might be more suitable for our study area, due to its longer wavelength, which will be less affected by the dense vegetation dominating the escarpment. Recent studies proved the suitability of SAOCOM imagery to measure displacements in the order of 6 cm/year (Roa et al., 2020).

5.2. Landslide-conditioning factors

The environmental conditions that better explained landslide occurrence in our study area combined topographic features and human disturbances. The influence of slope steepness, road construction and wildfires on slope instability was already acknowledged for the western slope of the Sierras Chicas (Beltramone, 2005). The AUC for both the training and testing datasets are considered excellent, according to Hosmer and Lemeshow (2000).

The positive relationship between slope steepness and landslide likelihood is related to the increasing influence of gravitational forces and is coincident with previous research (Conoscenti et al., 2015; Convertino et al., 2013; Gorsevski et al., 2006; Youssef et al., 2016). In our database, the average slope steepness of landslide presence points was 29° vs. 19° of non-landslide points, and 75% of landslides occurred at slopes steeper than 23°. According to Beltramone (2005), creeping processes are more frequent at milder slopes, rotational and translational landslides at intermediate slopes and rockfalls at steeper slopes (>35°). Similar results were observed in other mountain areas, reporting most landslides at slopes steeper than 15°–20° (García-Ruiz et al., 2010; Youssef et al., 2016) and around 30° (Lorente et al., 2003).

In addition, two human variables were also identified as favoring landslides on the western slope of the Sierras Chicas: road distance and fire frequency. The greater likelihood of landslides closer to roads is particularly related to the construction of El Cuadrado Road (E57) in 2011, involving slope cutting over disintegrated granite, schist and gneiss, and increasing their exposure to weathering agents (Figure S1 and S2). Since the road was inaugurated, we identified 24 landslides, including several rock failure events, associated with its construction. This instability represents a serious threat to road users and maintenance work is still necessary after eight years of road inauguration.

The positive role of fire frequency on landslide likelihood has been reported in this and other mountains, observing an increased number of landslides and reactivation of old ones after wildfires (Beltramone, 2005; Gartner et al., 2015; Highland and Bobrowsky, 2008; Ren et al., 2011). In our study area, fires eliminate most aerial biomass (Torres et al., 2014), thus reducing the interception of rainfall by the canopy and ultimately affecting hydromorphological processes of hillslopes, altering water flow partitioning and effective evapotranspiration which, in combination with reduced soil strength caused by root mortality, may contribute to slope instability (García-Ruiz et al., 2010; Gehring et al., 2019; Ren et al., 2011). Native woody species have shown high post-fire survival rates (Alinari et al., 2015; Torres et al., 2014); however, they

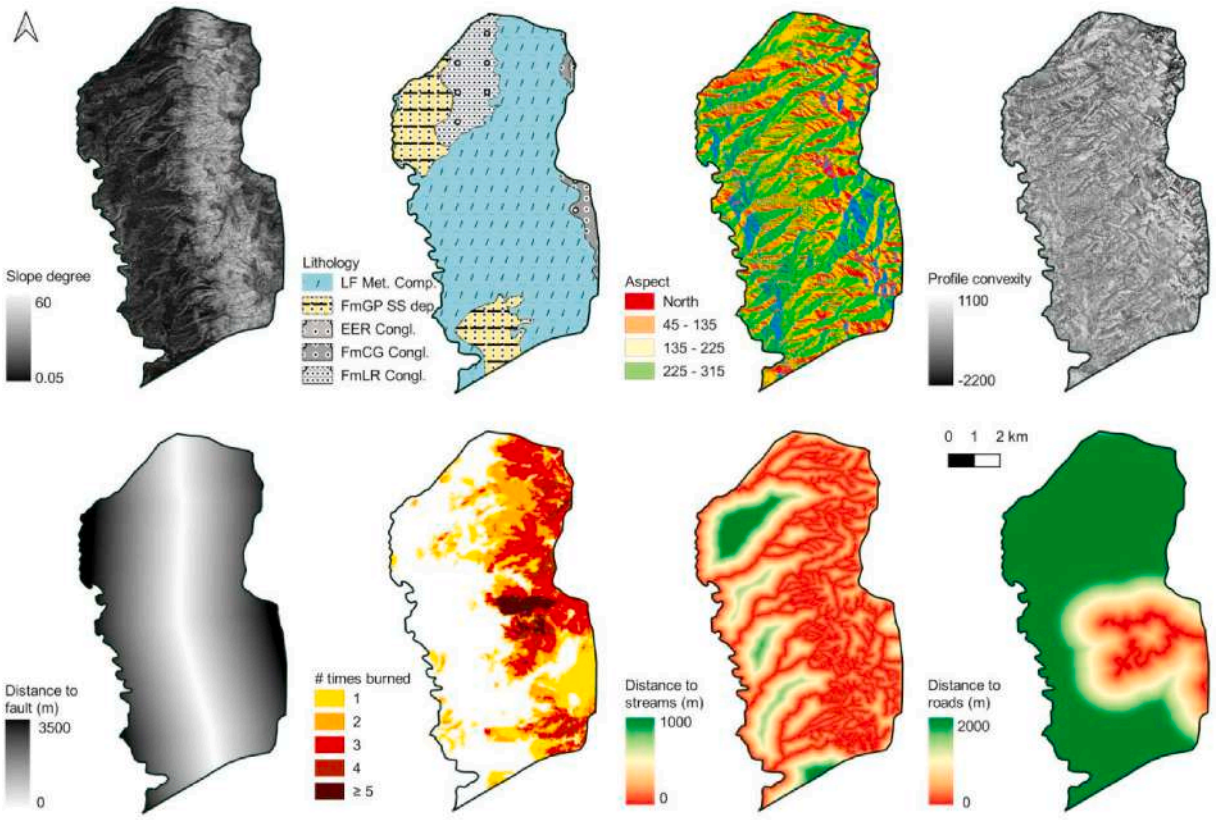

Fig. 8. Maps of independent variables included in the statistical analyses to identify landslide-conditioning factors in the Sierras Chicas mountains of central Argentina. LF Met Comp: La Falda Metamorphic Complex; Fm GP SS dep: Fm. General Paz Silt Sand deposit; EER Congl.: Estancia El Rosario, Conglomerate; FmCG Congl.: Fm Casa Grande, Conglomerate; FmLR Congl.: Fm Las Rabonas, Conglomerate.

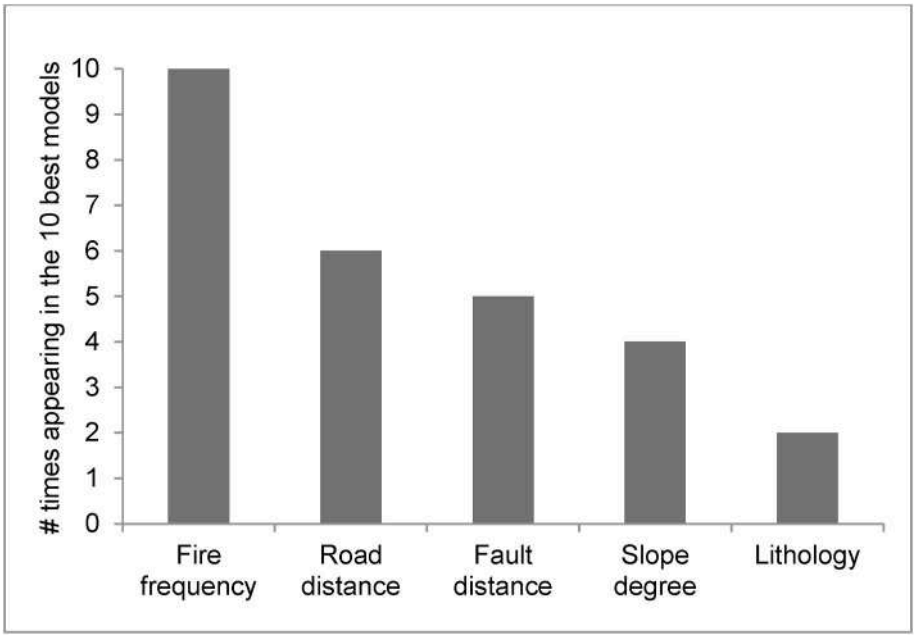

Fig. 9. Summary of best subset analyses to identify landslide-conditioning factors in Sierras Chicas (central Argentina). The y-axis indicates the number of times a variable was included in the best 10 models.

recover slowly and when wildfires are severe, survival is significantly reduced (Argibay and Renison, 2018). In addition, frequent fires promote early successional communities dominated by grasses and shrubs, which have greater flammability and burn more frequently than trees (Argañaraz et al, 2015, 2016, 2020). These recurrent fires prevent forest recovery, which provides soil strength greater than shrublands and grasslands (Chen et al., 2017; Zhang et al., 2016).

Besides the above-mentioned variables identified as conditioning

factors of landslides in our study area, there are other natural conditions suitable for landslides on the western slope of the Sierras Chicas, such as geomorphological dynamics, geology and soil characteristics (Beltramone, 2005). In addition, the precipitation regime is characterized by heavy rainfall events, directly associated with landslides (Beltramone, 2005). We believe that lithology was not identified as a significant predictor of landslides in our study because the available map was not detailed enough to provide significant variability (Fig. 1). Nevertheless, it was included in two of the ten best models (Fig. 9).

6. Conclusion

The implementation and use of interferometry among image pairs is a practical quantitative technique to monitor land surface displacements when data is scarce and its results are suitable for spatial analysis. Several limitations, as the availability of CSK images and suboptimal environmental settings, compromised the reliability of our results to accurately measure displacements. On the other hand, Sentinel-1 images provided better results for this area in terms of coherence, and they are potentially better to obtain more reliable displacement measurements in future studies, especially bearing in mind that their main acquisition mode is the Interferometric Wide (IW).

The environmental conditions that better explained landslide occurrence in our study area combined topographic features and human disturbances. The likelihood of landslides was higher in areas of steep slopes, close to roads (mainly El Cuadrado Road) and more frequently burned. Besides slope steepness, previous studies also reported other natural conditions suitable for landslide occurrence on the west hillside of the Sierras Chicas. This highlights the importance of avoiding human interventions increasing slope instability, such as road construction and recurrent wildfires. Forest expansion, via reforestation projects and fire prevention, can contribute to increase soil strength and reduce landslide hazard.

Our results will contribute to improving future applications of SAR interferometry in our study area and other areas with similar settings. This information represents a contribution to risk management and will help prevent improper decisions, like the construction of El Cuadrado road, across steep slopes and fragile substrate.

Author contribution

Conceptualization, Methodology, Software: ABM, JPA, MC, LB. Data curation,: ABM, AS, MD, JPA. Writing- Original draft preparation: JPA, ABM. Visualization, Investigation. JPA, CC, MC, MS: Supervision: JPA, MC, AS, MD, LB. Writing- Reviewing and Editing: ABM, JPA, AS, MD. Funding acquisition: JPA, MS

Declaration of competing interest

The authors declare that they have no known competing financial interests or personal relationships that could have appeared to influence the work reported in this paper.

Acknowledgments

This work was supported by the Ministry of Science and Technology of Córdoba Province (GRFT 2018). ABM has a PhD fellowship from SECyT-University of Córdoba. AS has a PhD fellowship from CONICET; LMB and JPA are researchers at CONICET. We also thank two anonymous reviewers and the Editor, whose comments helped to improve our manuscript. A. Brasca Merlin regards to European Academy of Bozen (Eurac research), especially Romy Schlogel, Giovanni Cuozzo and Claudia Notarnicola and to her master director of thesis Mario Lanfri and her colleagues Ignacio Pascual, Danilo Silva Griffouliere, Nicolas Madelón, Santiago Seppi and Verónica Andreo because science grows in collaboration. CSK SAR data was accessed through UEAT/CONAE, the unit for emergencies and early alerts from the Argentinean Space Agency within the framework of ABM master thesis from the Gulich Institute. Sentinel-1B data were freely downloaded from the ESA Sentinel Hub.

Appendix A. Supplementary data

Supplementary data to this article can be found online at https://doi.org/10.1016/j.jsames.2021.103179.

References

Alinari, J., von Muller, A., Renison, D., 2015. The contribution of fire damage to restricting high mountain Polylepis australis forests to ravines: insights from an unreplicated comparison. Ecol. Austral 25, 11–18.

Argañaraz, J.P., Cingolani, A.M., Bellis, L.M., Giorgis, M.A., 2020. Fire incidence along an elevation gradient in the mountains of central Argentina. Ecol. Austral 30, 268–281.

Argañaraz, J.P., Gavier Pizarro, G., Zak, M., Bellis, L.M., 2015. Fire regime, climate, and vegetation in the Sierras de Córdoba, Argentina. Fire Ecology 11, 55–73. https://doi.org/10.4996/fireecology.1101055.

Argañaraz, J.P., Landi, M.A., Bravo, S.J., Gavier-Pizarro, G.I., Scavuzzo, C.M., Bellis, L.M., 2016. Estimation of live fuel moisture content from MODIS images for fire danger assessment in Southern Gran Chaco. IEEE Journal of Selected Topics in Applied Earth Observations and Remote Sensing 9, 5339–5349. https://doi.org/10.1109/JSTARS.2016.2575366.

Argañaraz, J.P., Landi, M.A., Scavuzzo, C.M., Bellis, L.M., 2018. Determining fuel moisture thresholds to assess wildfire hazard: a contribution to an operational early warning system. PloS One 13 (10). https://doi.org/10.1371/journal.pone.0204889.

Argibay, D.S., Renison, D., 2018. Efecto del fuego y la ganadería en bosques de Polylepis australis (Rosaceae) a lo largo de un gradiente altitudinal en las montañas del centro de la Argentina. Bosque 39, 145–150. https://doi.org/10.4067/S0717-92002018000100014.

Barra, A., Monserrat, O., Mazzanti, P., Esposito, C., Crosetto, M., Scarascia Mugnozza, G., 2016. First insights on the potential of Sentinel-1 for landslides detection. Geomatics, Nat. Hazards Risk 7, 1874–1883. https://doi.org/10.1080/19475705.2016.1171258.

Bastarrika, A., Alvarado, M., Artano, K., Martinez, M.P., Mesanza, A., Torre, L., Ramo, R., Chuvieco, E., 2014. BAMS: a tool for supervised burned area mapping using Landsat data. Rem. Sens. 6, 12360–12380. https://doi.org/10.3390/rs61212360.

Bastarrika, A., Chuvieco, E., Martín, M.P., 2011. Mapping burned areas from Landsat TM/ETM+ data with a two-phase algorithm: balancing omission and commission errors. Rem. Sens. Environ. 115, 1003–1012. https://doi.org/10.1016/j.rse.2010.12.005.

Beltramone, C.A., 2005. Dinámica de las vertientes en la ladera Occidental de la Sierra Chica de Córdoba. Rev. Asoc. Geol. Argent. 60, 9–15.

Bianchini, S., Ciampalini, A., Raspini, F., Bardi, F., Di Traglia, F., Moretti, S., Casagli, N., 2015. Multi-temporal evaluation of landslide movements and impacts on buildings in san fratello (Italy) by means of C-band and X-band PSI data. Pure Appl. Geophys. 172, 3043–3065. https://doi.org/10.1007/s00024-014-0839-2.

Brasca Merlin, A., Mario, L., Claudio, C., Ignacio, P., Schlögel, R., Cuozzo, G., 2018. Remote sensing of landslides: guidelines for operative monitoring. In: 2018 IEEE Biennial Congress of Argentina (ARGENCON). IEEE, pp. 1–8.

Cabido, M., Zeballos, S.R., Zak, M., Carranza, M.L., Giorgis, M.A., Cantero, J.J., Acosta, A.T.R., 2018. Native woody vegetation in central Argentina: classification of Chaco and Espinal forests. Appl. Veg. Sci. 21, 298–311. https://doi.org/10.1111/avsc.12369.

Calò, F., Ardizzone, F., Castaldo, R., Lollino, P., Tizzani, P., Guzzetti, F., Lanari, R., Angeli, M.-G., Pontoni, F., Manunta, M., 2014. Enhanced landslide investigations through advanced DInSAR techniques: the Ivancich case study, Assisi, Italy. Rem. Sens. Environ. 142, 69–82. https://doi.org/10.1016/j.rse.2013.11.003.

Carignano, C.A., Cioccale, M.A., Martino, R.D., 2014. El megadeslizamiento del Cerro Uritorco, ladera Occidental de la Sierra Chica de Córdoba. Rev. Asoc. Geol. Argent. 71, 21–32.

Chen, W., Xie, X., Wang, J., Pradhan, B., Hong, H., Bui, D.T., Duan, Z., Ma, J., 2017. A comparative study of logistic model tree, random forest, and classification and regression tree models for spatial prediction of landslide susceptibility. Catena 151, 147–160. https://doi.org/10.1016/j.catena.2016.11.032.

Colesanti, C., Wasowski, J., 2004. Satellite SAR interferometry for wide-area slope hazard detection and site-specific monitoring of slow landslides. In: Proceedings Ninth Internat. Symposium on Landslides, pp. 795–802.

Conoscenti, C., Ciaccio, M., Caraballo-Arias, N.A., Gómez-Gutiérrez, Á., Rotigliano, E., Agnesi, V., 2015. Assessment of susceptibility to earth-flow landslide using logistic regression and multivariate adaptive regression splines: a case of the Belice River basin (western Sicily, Italy). Geomorphology 242, 49–64. https://doi.org/10.1016/j.geomorph.2014.09.020.

Convertino, M., Troccoli, A., Catani, F., 2013. Detecting fingerprints of landslide drivers: a MaxEnt model: fingerprints OF landslide drivers. J. Geophys. Res.: Earth Surface 118, 1367–1386. https://doi.org/10.1002/jgrf.20099.

Di Martire, D., Tessitore, S., Brancato, D., Ciminelli, M.G., Costabile, S., Costantini, M., Graziano, G.V., Minati, F., Ramondini, M., Calcaterra, D., 2016. Landslide detection integrated system (LaDIS) based on in-situ and satellite SAR interferometry

measurements. Catena 137, 406–421. https://doi.org/10.1016/j.catena.2015.10.002.
García-Ruiz, J.M., Beguería, S., Alatorre, L.C., Puigdefábregas, J., 2010. Land cover changes and shallow landsliding in the flysch sector of the Spanish Pyrenees. Geomorphology 124, 250–259. https://doi.org/10.1016/j.geomorph.2010.03.036.
Gartner, J.E., Santi, P.M., Cannon, S.H., 2015. Predicting locations of post-fire debris-flow erosion in the San Gabriel Mountains of southern California. Nat. Hazards 77, 1305–1321. https://doi.org/10.1007/s11069-015-1656-3.
Gehring, E., Conedera, M., Maringer, J., Giadrossich, F., Guastini, E., Schwarz, M., 2019. Shallow landslide disposition in burnt European beech (Fagus sylvatica L.) forests. Sci. Rep. 9 https://doi.org/10.1038/s41598-019-45073-7.
Giorgis, M.A., Cingolani, A.M., Gurvich, D.E., Tecco, P.A., Chiapella, J., Chiarini, F., Cabido, M., 2017. Changes in floristic composition and physiognomy are decoupled along elevation gradients in central Argentina. Appl. Veg. Sci. 20, 558–571. https://doi.org/10.1111/avsc.12324.
Gorsevski, P.V., Gessler, P.E., Foltz, R.B., Elliot, W.J., 2006. Spatial prediction of landslide hazard using logistic regression and ROC analysis. Trans. GIS 10, 395–415. https://doi.org/10.1111/j.1467-9671.2006.01004.x.
Hanssen, R.F., 2001. Radar Interferometry: Data Interpretation and Error Analysis. Springer Science & Business Media.
Herrera, G., Gutiérrez, F., García-Davalillo, J.C., Guerrero, J., Notti, D., Galve, J.P., Fernández-Merodo, J.A., Cooksley, G., 2013. Multi-sensor advanced DInSAR monitoring of very slow landslides: the Tena Valley case study (Central Spanish Pyrenees). Rem. Sens. Environ. 128, 31–43. https://doi.org/10.1016/j.rse.2012.09.020.
Highland, L., Bobrowsky, P.T., 2008. The landslide handbook: a guide to understanding landslides. US Geological Survey Reston.
Hooper, A., 2008. A multi-temporal InSAR method incorporating both persistent scatterer and small baseline approaches. Geophys. Res. Lett. 35.
Hosmer, D.W., Lemeshow, S., 2000. Applied Logistic Regression. John Wiley & Sons, New York.
Idrees, M.O., Saeidi, V., Pradhan, B., Yusuf, Y.A., 2013. Advanced differential interferometry SAR techniques for deformation monitoring: a review on sensors and recent research development. Geocarto Int.
Infante, D., Di Martire, D., Confuorto, P., Tessitore, S., Tòmas, R., Calcaterra, D., Ramondini, M., 2019. Assessment of building behavior in slow-moving landslide-affected areas through DInSAR data and structural analysis. Eng. Struct. 199, 109638. https://doi.org/10.1016/j.engstruct.2019.109638.
Kampes, B.M., 2006. Radar Interferometry. Springer.
Lasko, T.A., Bhagwat, J.G., Zou, K.H., Ohno-Machado, L., 2005. The use of receiver operating characteristic curves in biomedical informatics. Journal of Biomedical Informatics, Clinical Machine Learning 38, 404–415. https://doi.org/10.1016/j.jbi.2005.02.008.
Lencinas, A.N., 1971. Geologia del Valle de Punilla entre Bialet Masse y la Cumbre, provincia de Cordoba. Bol. Asoc. Geol. Cordoba 1, 61–70.
Lorente, A., Beguería, S., Bathurst, J.C., García-Ruiz, J.M., 2003. Debris flow characteristics and relationships in the Central Spanish Pyrenees. Nat. Hazards Earth Syst. Sci. 3, 683–691. https://doi.org/10.5194/nhess-3-683-2003.
Martino, R.D., Guereschi, A.B., Carignano, C.A., 2012. Influencia de la tectónica preandina sobre la tectonica andina: el caso de la falla de la Sierra Chica, Sierras Pampeanas de Córdoba. Rev. Asoc. Geol. Argent. 69, 207–221.
Massabie, A., Sanguinetti, A., Lo Forte, G., Cegarra, M., 2003. La actividad neotectónica en la sierra Baja de San Marcos-Cruz del Eje, flanco Occidental de las Sierras Pampeanas Orientales. Rev. Asoc. Geol. Argent. 58, 653–663.
Moreiras, S.M., Coronato, A., 2009. Landslide processes in Argentina. Dev. Earth Surf. Process 13, 301–332.
Nutricato, R., Nitti, D.O., Bovenga, F., Refice, A., Wasowski, J., Chiaradia, M.T., Milillo, G., 2015. COSMO-SkyMed multi-temporal SAR interferometry over liguria region for environmental monitoring and risk management. In: 2015 IEEE International Geoscience and Remote Sensing Symposium (IGARSS). Presented at the 2015 IEEE International Geoscience and Remote Sensing Symposium. IGARSS, pp. 1405–1408. https://doi.org/10.1109/IGARSS.2015.7326040.
Pappalardo, G., Mineo, S., Angrisani, A.C., Di Martire, D., Calcaterra, D., 2018. Combining field data with infrared thermography and DInSAR surveys to evaluate the activity of landslides: the case study of Randazzo Landslide (NE Sicily). Landslides 15, 2173–2193. https://doi.org/10.1007/s10346-018-1026-9.
Quinn, G.P., Keough, M.J., 2002. Experimental Design and Data Analysis for Biologists. Cambridge University Press.
R Core Team, 2020. R: a Language and Environment for Statistical Computing. R Foundation for Statistical Computing, Vienna, Austria.
Ren, D., Fu, R., Leslie, L.M., Dickinson, R.E., 2011. Modeling the mudslide aftermath of the 2007 southern California wildfires. Nat. Hazards 57, 327–343. https://doi.org/10.1007/s11069-010-9615-5.
Richardson, T., Gilbert, H., Anderson, M., Ridgway, K.D., 2012. Seismicity within the actively deforming eastern Sierras Pampeanas, Argentina. Geophys. J. Int. 188, 408–420.
Roa, Y., Rosell, P., Solarte, A., Euillades, L., Carballo, F., García, S., Euillades, P., 2020. First assessment of the interferometric capabilities of SAOCOM-1A: new results over the domuyo volcano, neuquén Argentina. J. S. Am. Earth Sci. https://doi.org/10.1016/j.jsames.2020.102882, 102882.
Rozos, D., Pyrgiotis, L., Skias, S., Tsagaratos, P., 2008. An implementation of rock engineering system for ranking the instability potential of natural slopes in Greek territory. An application in Karditsa County. Landslides 5, 261–270. https://doi.org/10.1007/s10346-008-0117-4.
Torres, R.C., Giorgis, M.A., Trillo, C., Volkmann, L., Demaio, P., Heredia, J., Renison, D., 2014. Post-fire recovery occurs overwhelmingly by resprouting in the Chaco Serrano forest of Central Argentina: post-fire tree regeneration. Austral Ecol. 39, 346–354. https://doi.org/10.1111/aec.12084.
Varnes, D.J., 1978. Slope movement types and processes. Special report 176, 11–33.
Wasowski, J., Bovenga, F., 2014. Investigating landslides and unstable slopes with satellite Multi Temporal Interferometry: current issues and future perspectives. Eng. Geol. 174, 103–138.
Youssef, A.M., 2015. Landslide susceptibility delineation in the Ar-Rayth area, Jizan, Kingdom of Saudi Arabia, using analytical hierarchy process, frequency ratio, and logistic regression models. Environmental earth sciences 73, 8499–8518.
Youssef, A.M., Pourghasemi, H.R., Pourtaghi, Z.S., Al-Katheeri, M.M., 2016. Landslide susceptibility mapping using random forest, boosted regression tree, classification and regression tree, and general linear models and comparison of their performance at Wadi Tayyah Basin, Asir Region, Saudi Arabia. Landslides 13, 839–856. https://doi.org/10.1007/s10346-015-0614-1.
Zêzere, J.L., Pereira, S., Melo, R., Oliveira, S.C., Garcia, R.A.C., 2017. Mapping landslide susceptibility using data-driven methods. Sci. Total Environ. 589, 250–267. https://doi.org/10.1016/j.scitotenv.2017.02.188.
Zhang, G., Cai, Y., Zheng, Z., Zhen, J., Liu, Y., Huang, K., 2016. Integration of the statistical index method and the analytic hierarchy process technique for the assessment of landslide susceptibility in huizhou, China. Catena 142, 233–244. https://doi.org/10.1016/j.catena.2016.03.028.
Zhao, C., Zhang, Q., He, Y., Peng, J., Yang, C., Kang, Y., 2016. Small-scale loess landslide monitoring with small baseline subsets interferometric synthetic aperture radar technique—case study of Xingyuan landslide, Shaanxi, China. J. Appl. Remote Sens. 10, 026030 https://doi.org/10.1117/1.JRS.10.026030.